land

MDPI

Article

Production–Living–Ecological Spatial Function Identification and Pattern Analysis Based on Multi-Source Geographic Data and Machine Learning

Ziqiang Bu [1,2], Jingying Fu [1,2,*], Dong Jiang [1,2,3] and Gang Lin [1,2,*]

[1] Institute of Geographic Sciences and Natural Resources Research, Chinese Academy of Sciences, Beijing 100101, China; buziqiang3314@igsnrr.ac.cn (Z.B.); jiangd@igsnrr.ac.cn (D.J.)
[2] College of Resources and Environment, University of Chinese Academy of Sciences, Beijing 100049, China
[3] Key Laboratory of Carrying Capacity Assessment for Resource and Environment, Ministry of Natural Resources, Beijing 100101, China
* Correspondence: fujy@igsnrr.ac.cn (J.F.); ling@lreis.ac.cn (G.L.); Tel.: +86-010-6488-9221 (J.F.); +86-188-1175-9109 (G.L.)

Abstract: Land use cannot be simply understood as land cover. The same land may carry different functions, such as production, living, and ecological applications; the dominant function of land will affect and restrict other uses. Disorderly urbanization and industrialization have led to an intensification of conflicts among the production, living, and ecological functions of land, which is a major constraint on regional sustainable development. This paper took the perspective of land-use function and used multi-source data such as Sentinel remote-sensing imagery, VIIRS night-time light data, and POIs to classify land-use functions on a large scale in the Beijing–Tianjin–Hebei (BTH) urban agglomeration. The specific research process was as follows. Firstly, the BTH region was multi-scale-segmented based on Sentinel remote-sensing data. Then, the spectral, texture, shape, and socio-economic features of each small area after segmentation were extracted. Moreover, a PLES land-use classification system oriented towards land-use function was established, and a series of representative samples were selected. Subsequently, a random forest model was trained using these samples; then, the trained model was used for the large-scale analysis of land use in the entire BTH region. Finally, the spatial distribution patterns and temporal–spatial evolution characteristics of PLES in the BTH region from 2016 to 2021 were analyzed from the macro level to the micro level.

Keywords: multi-source data; multi-scale segmented; PLES; random forest

Citation: Bu, Z.; Fu, J.; Jiang, D.; Lin, G. Production–Living–Ecological Spatial Function Identification and Pattern Analysis Based on Multi-Source Geographic Data and Machine Learning. *Land* **2023**, *12*, 2029. https://doi.org/10.3390/land12112029

Academic Editors: Yinghui Zhang, Jingzhe Wang, Yangyi Wu, Ivan Lizaga and Zipeng Zhang

Received: 6 October 2023
Revised: 5 November 2023
Accepted: 5 November 2023
Published: 7 November 2023

1. Introduction

The problems caused by urbanization and industrialization, such as resource constraints, unbalanced urban–rural development, and increased risks to food security, are constantly deteriorating. Land-use conflicts between various stakeholders are intensifying, and interactions between production, living, and ecological spaces are gradually becoming unbalanced [1,2]. For example, the development of farmland and the construction of factories continue to encroach on living and ecological spaces, in the same time, The disorderly expansion of urban residential buildings and the large number of new buildings in the countryside have encroached on cultivated land and ecological land to some extent. On the contrary, the occupied and destroyed ecological space may have negative feedback on the production space and living space by natural disasters such as landslide and sand storm and the reduction in ecological service value. It can be seen that the rational layout of production, living, and ecological spaces and the balanced play of their functions are important contents in realizing sustainable land use. From a realistic perspective, with the development and growth of urban scale, cities are connected into urban agglomerations, and the flow of production, living, and ecological factors within urban agglomerations

is very close. The functional changes in land use in different cities may have similar laws or mutual influences [3]. Therefore, identifying the land-use patterns of cities and urban agglomerations from the perspective of function can elucidate the dynamic changes in and impacts between the production, living, and ecological functions of land during urbanization and industrialization, so as to evaluate and diagnose the sustainability of land use.

Traditional land-use classification mainly identifies land cover through the spectral, textural, and other advanced features of remote-sensing images. These can mainly be divided into the following three categories: pixel-based classification methods, object-oriented classification methods, and scene-based classification methods [4]. Various classification methods are applicable to different remote-sensing image features. Pixel-based classification methods mainly analyze differences in the spectral information of pixels for classification. Some simpler machine-learning methods are being trialed that do not require many input features [5–7]; they are suitable for low- and medium-resolution remote-sensing images. For example, Fei Yuan et al. used the maximum likelihood method to classify most of the Minnesota urban area pixel by pixel in tandem with multi-temporal Landsat series data, and quantified the land-cover change patterns of the city with an overall classification accuracy between 80% and 90% [8]. However, pixel-based classification methods neglect the shape and texture features of land cover, and are constrained by the "spectral confusion" issue, which may lead to misclassification and omission errors of land cover [9,10]. Object-based image analysis (OBIA) uses geographic objects as the basic unit for land-cover classification [11,12], which reduces intra-class variation and eliminates the salt-and-pepper effect caused by misclassification. The advantage of OBIA is that it incorporates various information sources, enabling the use of the texture, shape, and location of feature objects as the basis for classification [13–15], which can reveal more image information. For example, Mengmeng Li et al. applied OBIA classification methods, bifurcated segmentation trees, and energy minimization algorithms to the image segmentation of very-high-resolution (VHR) satellite images, which can effectively distinguish buildings from other man-made objects [16]. Scene-based land-use classification, mainly utilizing convolutional neural network methods, is suitable for extracting deep image features from ultra-high-resolution images [17]. For example, Nimrabanu Memon et al. applied CNNs for the automatic land-cover classification of multi-resolution dual-polarized data and found that CNN models trained on low-spatial-resolution images were more adept at performing migration learning to predict higher-resolution images [18]. Recently, the demand for the fine-grained planning of functional areas within major urban areas and the increasing availability of socioeconomic big data (SBD) have given rise to a boom in fusing high-resolution remote-sensing imagery and SBD for urban functional area identification [19–23]. For example, Feng et al. proposed a scene–object–economy recognition framework that fuses building vectors, POIs, and high-resolution remote-sensing image features to compensate for the inability of remote-sensing images to mine 3D features [24]. However, the difficulty of data acquisition and the incoherence of data have created bottlenecks in this field of research, because higher-resolution remote-sensing satellites tend to have long re-entry cycles and are costly and expensive to acquire. In addition, convolutional neural networks can be expensive in terms of hardware costs and time costs for training and prediction [25]. Therefore, it is difficult to apply scenario-based land-use classification and urban functional area identification to large-scale land-use mapping. Taken together, the OBIA approach has a higher accuracy than image-based detection methods [26], and it is more feasible than approaches using scenario-based and multi-source data in the field of long time series large-scale land-use mapping; In addition, the OBIA approach can be used in conjunction with complex machine-learning algorithms, and the influence of input variables on the results can be analyzed after the results are produced which makes it more suitable for large-scale, multi-feature input land-use classification. Taken together, all three classification methods apply machine-learning algorithms for classification to a greater or lesser extent, due to the fact that machine-learning models, which can be based on features extracted from

classification objectives and manually given labels, have become an indispensable process for automated land-use classification.

The function of production–living–ecological space (PLES) refers to the characteristics or functions displayed by different types of national spatial areas in terms of residents' production and living activities under the joint influence of internal composition elements and external influencing factors, forming a complex community in terms of economic, social, and geographic elements. The rational layout and balanced functioning of PLES is important for coordinated regional development and sustainable land use. However, few existing classification studies have used PLES as a classification system. Existing relevant research mainly uses the merged classification method [27–29] and the index system measurement method [30–32] to identify PLES based on existing publicly available land-use products. For example, Li et al. constructed a classification system for urban PLES functions using the index system measurement method from a comprehensive perspective of land function, ecosystem services, and landscape functions, and integrated spatial function value accounting functions based on ecosystem service value evaluation. They determined the dominant type of spatial function through vertical and horizontal comparisons [33]. While Nan et al. used the merged classification method to produce the spatial and temporal distribution data of PLES in Xinjiang from 2000 to 2020, the center of gravity transfer model and Moran's I method were used to analyze and summarize its distribution pattern and spatio-temporal evolution [34].

However, both of these methods used in most of the PLES classification studies are overly dependent on traditional land-use classification products and have certain limitations: Firstly, traditional land-use classification products do not take into account the functionality of the land use; for example, they cannot differentiate between factories, subdivisions, and rural home sites. And publicly available land-use products are limited in their accuracy and have a resolution that is difficult to satisfy. Therefore, a small number of studies has begun to focus on directly dividing land functions based on the PLES classification system from socioeconomic or remote-sensing data. For example, using POIs as the data source, Fu et al. effectively identified PLES in the central urban area of Wuhan, China, revealing influencing factors through the application of the analytic hierarchy process (AHP), spatial analysis, and quadrat proportion method [35]. However, due to data limitations, these studies are predominantly limited to the main urban areas of a single city and cannot consider the impact of rural living space, agricultural production space, and ecological land outside the city on the distribution and combination patterns of functional urban PLES. In addition, previous studies have been unable to characterize the interactions of PLES functions among different cities within an urban agglomeration. Therefore, it is necessary to classify land based on PLES functions at a larger scale, which encompasses complex geographic areas with diverse geographic environments and socio-economic activities such as the urban agglomeration scale. This study took the Beijing–Tianjin–Hebei city cluster (BTH) as the study area, adopted a PLES classification system based on a functional perspective, used POI data with long time series and night-time lighting data to assist, and employed a classification algorithm with object-oriented integrated machine-learning (random forest) for the large-scale land-use mapping of Sentinel images in order to provide more reliable basic data (10 m resolution) for researchers to conduct subsequent research on land issues.

2. Materials and Methods

2.1. Study Area

The Beijing–Tianjin–Hebei city cluster(Figure 1) located at latitude 37°27′~42°40′ N and longitude 113°27′~119°50′ E, is situated in the area north of the lower reaches of the Yellow River in northern China, east of the Bohai Sea, including the 2 municipalities directly under the central government of Beijing and Tianjin, and 11 prefecture-level cities such as Shijiazhuang and Tangshan in Hebei province, with a land area of approximately 180,000 km^2, accounting for 3.8% of the total urban land area of the country. BTH is

situated within the temperate continental monsoon climate zone, with high topography in the northwest and low topography in the southeast; the arable land is generally devoted to dryland farming. The BTH region, which has a high population density, a long history of agriculture, and rapid industrial development, is the largest urban agglomeration in the Bohai Sea region of Northeast Asia, and it is the largest and most dynamic economic zone in northern China. Separately, Beijing is the economic, political, and cultural center of China, with an important development status, and is a city of significant status in China. Tianjin is located in the center of the Bohai Sea region, and has a port known as "the largest port in northern China". Tianjin is also the economic hinterland of the Beijing–Tianjin–Hebei region, with a vast land area, abundant natural resources, and developed high-tech industries, which has enormous potential for development. Hebei province, located in the heart of the Bohai Sea region, contains 11 prefecture-level cities. It has tremendous development advantages in terms of natural resources, distribution, production, markets, talents, and location, making it one of the fastest-growing economic regions in China. In recent years, Beijing and Tianjin, as the central growth points of the region, have stimulated the integrated development of sub-cities in the region, enabling the BTH to achieve a regional GDP of RMB 9.6 trillion in 2021 [36,37]. However, the siphoning effect of large cities has led to unbalanced development within the BTH, exhibiting polarization; rapid urbanization and industrialization have led to ecological degradation, reductions in arable land area, traffic congestion, and deterioration of the population's living environment, which affects sustainable economic and social development [38]. The rapid development of non-agriculturalization in rural areas of the BTH region has been attributed to the advancement of urbanization and industrialization. This has also resulted in a strong transition of rural production spaces and living spaces towards urban production and living spaces, causing certain encroachment and damage to ecological spaces in the process. However, research on the distribution and evolution of land-use functions in the BTH from a PLES perspective is relatively scattered. Therefore, this study selected the BTH region as the study area to investigate the functional utilization of land use at different scales, which has typical significance.

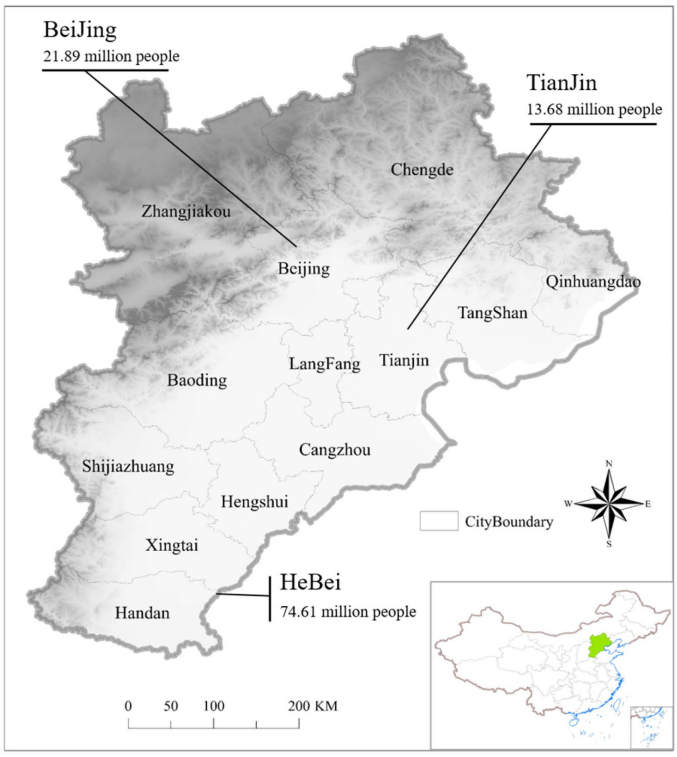

Figure 1. Study area location.

2.2. Research Data

2.2.1. Sentinel-2A Remote-Sensing Data

Sentinel-2A has 13 bands with a width of 290 km and a revisit period of 10 d. The remote-sensing images for this study were downloaded from the Google Earth Engine platform (https://earthengine.google.com/ (accessed on 20 February 2023)), and the images were collected during the crop-growing periods of 2016 and 2021 (1 April to 31 October). Additionally, pre-processing steps such as image de-clouding, cropping, mosaic, mean fusion, etc., were completed online by means of code on the platform, and four bands of red, green, blue, and near-infrared were screened.

For the spectral features required for the study, the red, green, blue, and near-infrared bands of Sentinel-2A were fused by interrogating the built-in module of the Google Earth Engine (GEE) platform; then, the texture features were extracted according to the principal component bands to obtain 18 texture features of the principal component bands within the BTH. The corner second-order, correlation, and entropy texture features were finally determined by feature analysis moment, correlation, and entropy as the classification features.

2.2.2. Night-Time Lighting Data and POI Data

Night-light remote sensing is recognized as a good data source for the large-scale simultaneous monitoring of socioeconomic activities and has been widely used in the fields of population estimation, economic estimation, urbanization monitoring, and energy consumption studies [39]. The spatial resolution of NPP/VIIRS is 15″ at the monthly scale; this sensor has a sensitive perception of faint lights at night across a long time series. In this study, the annual synthesis, cropping, and mosaic visualization of these data were accomplished using the Google Earth Engine platform. POI data refer to points of interest, which record the name, category, latitude, and longitude of various activities on the ground and other basic information. It has been shown that POI data can effectively describe the function of a plot [40]. In this study, Python was used to crawl POI data of 13 cities in the BTH for 2016 and 2021 from the Baidu map platform, and then convert POIs from vector point data to raster density data and resample them to a 10 m resolution through kernel density analysis in the ArcGIS platform to perform the fusion analysis of multi-source data.

The final acquired features and data sources are shown in Table 1, where the shape features are the area, perimeter, and structure ratio of the object after object-oriented multiscale segmentation. Spectral features and texture features are used to distinguish different subsurface types, which are often used in traditional studies; whereas shape features and socioeconomic features are added to our algorithm, which help to distinguish different building categories for the PLES functional identification, which is the innovation of this paper.

Table 1. Classification features and data source.

Feature Type	Bands	Data Source
Spectral features	B8	Sentinel-2A
	B4	Sentinel-2A
	B3	Sentinel-2A
	B2	Sentinel-2A
	NDVI	Sentinel-2A
Shape features	Area	Object segmentation
	Perimeter	Object segmentation
Texture features	Structure ratio	Object segmentation
	Second-order moment	GEE
	Relevance	GEE
	Entropy	GEE
Socioeconomic features	Night light value	NPP/VIIRS
	POIs density	Nucleation density of POIs

2.3. Research Methods

This paper proposes a large-scale land-use identification method using a production–living–ecological network as the classification system, which can represent the functionality of land use. In concrete terms, object-oriented segmentation on remote-sensing images was performed first. After completing the segmentation, the segmented objects were converted into vector polygons, and the subsequent extraction of features and selection of samples and labels are based on the vector polygons after object-oriented segmentation. Then, we extracted the spectral, shape, texture, and socioeconomic features of each pixel within the object from Sentinel optical images, NPP/VIIRS night-time lighting images, and POI data and constructed a PLES spatial classification system. Subsequently, some representative samples for labeling were selected. These samples were used to extract features from multi-source data, and the optimal random forest model was trained by adjusting each parameter. Finally, the trained models were used to perform large-scale classification on the whole area of the study area. The specific research process is shown in Figure 2.

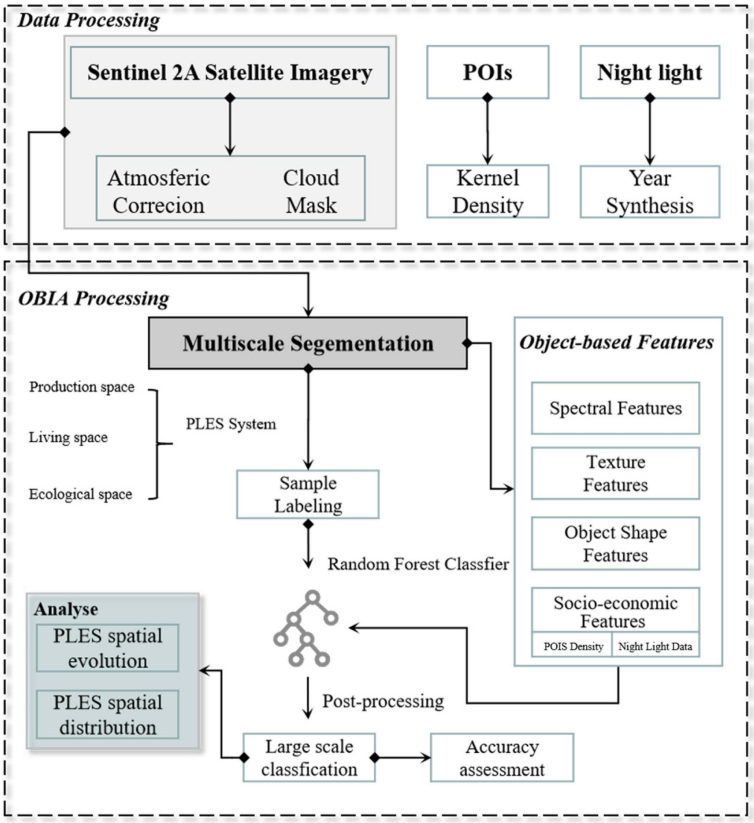

Figure 2. Technical framework.

2.3.1. PLES Spatial Classification System

Traditional land-use classification is mostly based on land-cover discrimination, using remote-sensing image features to discriminate ground attachments for land-use classification; however, land is an integrated functional whole, and its production, living, and ecological functions are interlinked. In this study, a PLES classification system (Table 2) was constructed that considers the surface cover and land-use functionality, and divides the regional land into three primary classifications and nine secondary classifications. This is important for analyzing functional PLES conflicts and the coupling characteristics of city clusters, and studying the sustainable development of urban clusters. This classification system is important for analyzing the conflict and coupling characteristics of the PLES functions of city clusters and studying the sustainable development of urban agglomerations.

Table 2. PLES classification system.

Level 1 Classification	Level 2 Classification	Code
Production area	Agricultural space	11
	Industrial space	12
	Transportation space	13
Living area	Rural living space	21
	Urban living space	22
Ecological area	Waters	31
	Urban ecological space	32
	Non-urban ecological space	33
	Unused space	34

2.3.2. Object-Oriented Multi-Scale Segmentation Algorithm

The object-oriented multi-scale segmentation algorithm views an image as a neighborhood graph consisting of topological relationships between sub-regions and within an image region [41]. Starting from a single image element card, segmentation is performed according to a specified scale, and adjacent image regions are merged and grown two by two. To ensure that the merged regions have a high degree of homogeneity, it is necessary to set a threshold to control the process of patch growth so as to segment feature objects at the optimal scale. The basic idea of the algorithm is that starting from a single image element, the difference metrics are calculated separately with the neighboring image elements, and merging is carried out within the allowed range of the heterogeneity threshold; after the completion of one round of merging, objects generated in the previous round are used as the basic unit, and calculations are continued separately with the neighboring objects; the above steps are iterated until no more objects can be merged under the specified heterogeneity threshold.

The heterogeneity between objects consists of spectral heterogeneity and shape heterogeneity. Initially, each pixel is treated as a region, and the disparity metric (f) is calculated.

$$f = w_1 x + (1 - w_1) y \tag{1}$$

where w_1 is the weight value, $0 \leq w_1 \leq 1$, x is the spectral heterogeneity, and y is the shape heterogeneity. The spectral heterogeneity and shape heterogeneity methods are expressed as follows:

$$x = \sum_{i=1}^{n} p_i \sigma_i \tag{2}$$

$$y = w_2 u + (1 - w_2) v \tag{3}$$

where p_i is the weight of the ith image layer, σ_i is the standard deviation of the spectral value of the ith image layer, u is the overall tightness of the image area, v is the smoothness of the image area boundary, and w_2 is the weight, $0 \leq w_2 \leq 1$. The formula for the calculation is:

$$u = E/\sqrt{N} \tag{4}$$

$$v = E/L \tag{5}$$

where E is the actual boundary length of the image area, N is the total number of image elements in the image area, and L is the total length of the rectangular boundary containing the extent of the images.

2.3.3. Random Forest Classification Algorithm

Random forest is a machine-learning algorithm proposed by Breiman et al. [42]; it is an integrated learning algorithm in which multiple decision trees are integrated together for decision making. A random forest consists of numerous decision trees, each of which grows independently and forks at nodes with randomly selected parameters of the characteristic

variables, and the final prediction results are selected by each decision tree. Decision tree models are usually tuned by the number of iterations of decision trees and the number of feature parameters contained in each tree. After sampling the data in random forests, the features are also randomly sampled to ensure independence of the predictor; thus, random forest systems can handle a large amount of high-dimensional data and can determine the interactions between various features. In this study, multi-source data from 2016 and 2021 were collected, and then the same sample points were used to extract objects, shapes, and socioeconomic features from these two periods of data, respectively. And through field research and manual visual interpretation, labels were set according to the actual functional land-use changes, and the resulting datasets were used to train two different random forest models. During the training process, iterating the three hyperparameters of the depth of the decision tree in a random forest, the maximum number of features, and the minimum number of samples contained in the leaf nodes was specially focused on.

3. Results

3.1. Object-Oriented Segmentation and Accuracy Evaluation of the Random Forest Algorithm

In this study, the GEE platform was first used to perform the atmospheric correction, cloud removal, clipping, and mosaicking of Sentinel images at different times in the study area, and calculate texture features. Then, downloaded images of the BTH region were subjected to multi-scale segmentation using ArcGIS Pro 2.8 software and Python programs. After segmentation, 1956 sample points were selected in the BTH region through visual interpretation, considering the surface coverage and land-use function, covering three primary classifications and nine secondary classifications, and fully considering the characteristics of developed and undeveloped areas within the urban agglomeration. The spectral, shape, textural, and socio-economic features of these samples were then extracted as input data and fed into the random forest algorithm for training. By calculating the confusion matrix of the classification results for different schemes, the classification accuracy of each category and the overall classification accuracy could be obtained.

Specifically, in order to test and validate that the combination of spectral, shape, textural, and socio-economic features is more conducive to functionally oriented PLES classification, three different training plans were implemented, including Plan A, using only Sentinel spectral and textural features; Plan B, using remote-sensing features and object-based segmented shape features; and Plan C, using a combination of spectral features. As shown in Table 3. The overall accuracy rates of Plan A, Plan B, and Plan C were 85.06%, 87.64%, and 93.97%, respectively. The Kappa coefficients were 82.66, 85.74, and 92.98, respectively. It can be seen that as the number of features involved in the classification gradually increased, the classification accuracy was gradually improved to a certain extent.

In Plan A, the results obtained using only remote-sensing image features for classification were poor, especially due to the confusion between urban living space and rural living space, as well as urban green space and non-urban green space, because these two groups of land-cover types were only distinguished through the land-use function and had similar visual effects in land cover, which may have caused "same spectrum different object" and "same object different spectrum" phenomena in the spectral domain. After adding shape features (Plan B), this problem was somewhat improved, with an overall accuracy improvement of 2.58%. Shape features help to identify subtle differences between certain land-cover types from other dimensions. For example, agricultural production spaces and rural living spaces on the North China Plain generally exhibit regular shapes, while living spaces in urban areas have larger patch areas, and road land appears elongated. In Plan B, the prediction accuracy of industrial production spaces increased by 4%, and the prediction accuracy of road land increased by 8%. However, the misclassification phenomenon between the main urban area and the non-main urban area remained significant.

Table 3. Classification accuracy of different plans.

	Plan A				Plan B				Plan C			
	PA/%	**UA/%**	**OA/%**	**Kappa**	**PA/%**	**UA/%**	**OA/%**	**Kappa**	**PA/%**	**UA/%**	**OA/%**	**Kappa**
Agricultural space	0.87	0.89			0.82	0.98			0.98	0.96		
Industrial space	0.89	0.96			0.93	0.96			0.93	1.00		
Transportation space	0.76	0.76			0.94	0.61			0.89	0.89		
Rural living space	0.89	0.91			0.90	0.93			0.97	0.97		
Urban living space	0.90	0.86	85.06	82.66	0.89	0.96	87.64%	85.74%	1.00	0.96	93.97	92.98
Waters	0.95	0.93			1.00	0.91			0.84	0.84		
Urban ecological Space	0.68	0.73			0.75	0.77			0.94	1.00		
Non-urban ecological space	0.53	0.47			0.77	0.67			0.79	0.81		
Unused space	0.86	0.60			0.83	0.62			1.00	0.57		

In Plan C, both night-time light features and POI density were added, which could effectively distinguish urban central areas from non-urban areas (urban central areas generally exhibit a high economic activity density, numerous POIs, and high night-time light brightness, while suburbs are the opposite). This led to an overall accuracy increase of 6.33% and a Kappa coefficient increase of 7.24, greatly improving the model's ability to distinguish between urban and agricultural living spaces, urban green spaces, and non-urban ecological green spaces. The confusion matrix of the validation set for Plan C is shown in Figure 3, which indicates that the overall performance of the algorithm and dataset is good, but errors still occur in distinguishing between roads and agricultural living land and between agricultural production space and non-urban green space. To some extent, the shape features obtained from object-oriented segmentation and the socio-economic features provided by night-time light and POI density data help to solve the problems of "same object, different spectrum" and "same spectrum, different object" (which is more typical in function-type classification) and can significantly improve the accuracy of the spatial classification of PLES based on functionality.

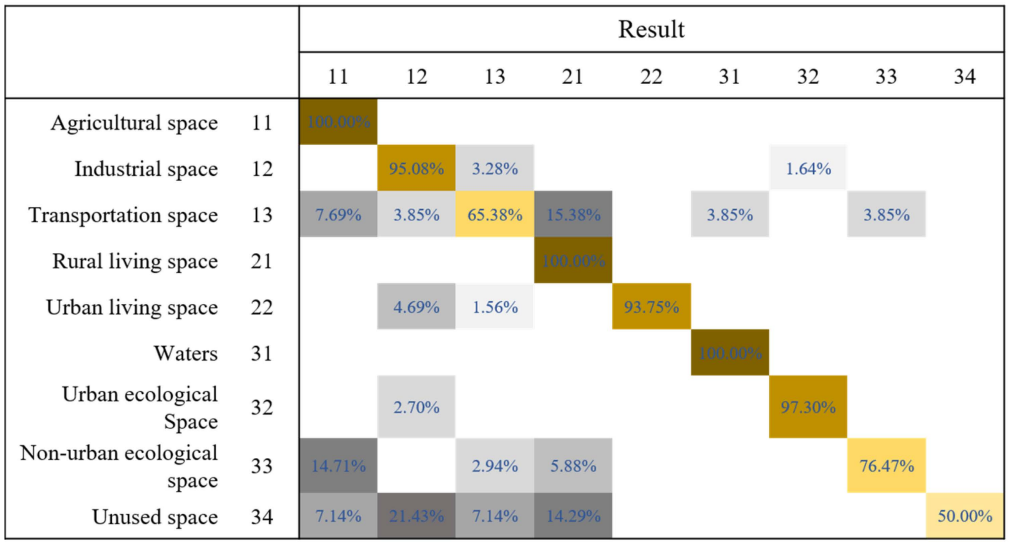

Figure 3. Confusion matrix on the validation set of the dataset in 2021 (Warm colors indicate correct classification, while gray indicates incorrect classification).

In addition, the representativeness of the selected samples is important for PLES classification at such a large scale (the BTH region). Therefore, Google imagery, Sentinel imagery, and other base maps were utilized to validate the accuracy of the large-scale land-use classification data obtained from the Plan-C-based trained model. We randomly selected a portion of the validation points and obtained an accuracy of only 84.17%, which can meets the needs of large-scale land-use analysis, although the actual accuracy has decreased to a certain extent compared with the accuracy on the model validation set.

The above results indicate that the feature set composed of spectral, texture, shape, and socioeconomic features can effectively train a model for fine-grained PLES classification. To evaluate the numerous features extracted from multi-source data, the contribution rates of each feature to the classification results were calculated (as shown in Figure 4a). Among the 23 features, there is a significant difference in the contribution rates of each feature to the classification results (spectral features contributed a total of 57.8%, while texture features, shape features, and socio-economic features cumulatively contributed 19.0%, 5.6%, and 17.6%, respectively). Specifically, the average value of the red band from Sentinel in the spectral features demonstrated the highest contribution rate: approximately 13.53%. Additional features with high contribution rates included the average NDVI value of land objects and the average night-time light brightness of land objects. Although some textural and shape features have relatively low contribution rates, they still play a positive role in improving the accuracy of the final classification.

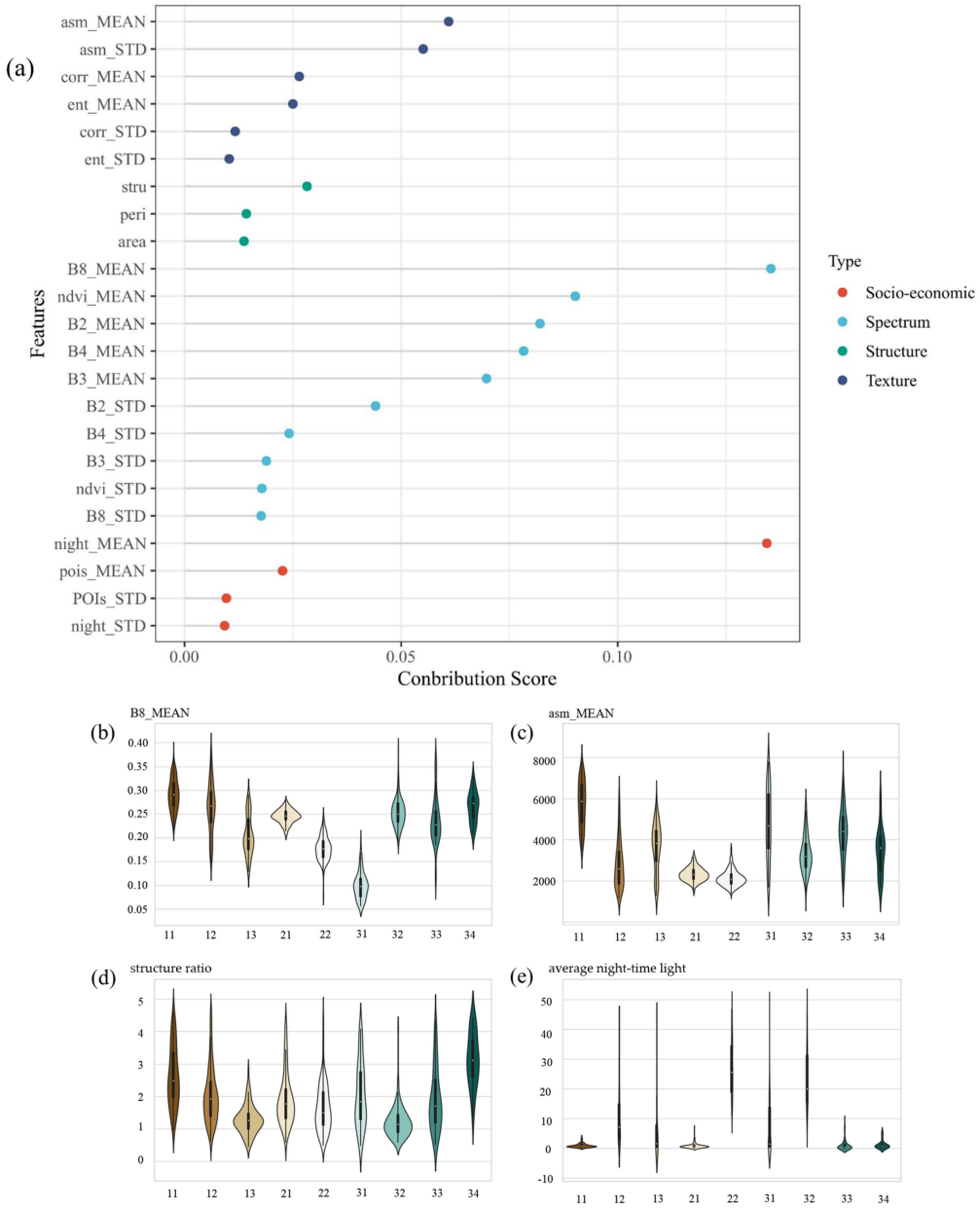

Figure 4. (**a**) Contribution of each feature to the final classification model; (**b**–**e**) Distribution of the values of the four typical features at the sample points.

To specifically explore the discriminative effect of different features on PLES categories, the feature values of typical four categories were computed (as shown in Figure 4b–d): the average red band value of each object (B8_MEAN refers to the mean of the red band values of all image elements of an object, which is a typical representative of spectral features); the average value of the angle second-order moment band (asm_MEAN is the mean of angular second-order moments of all image elements of an object, which is a typical representative of texture features); the structure ratio (the more prominent shape feature); and the average night-time light brightness (the more prominent socio-economic feature) of each object. These four categories represent spectral, textural, shape, and socioeconomic features, respectively. Different land covers have different observable reflectance values in the red band, with vegetation exhibiting the highest values, followed by buildings and water bodies. The red band also aids in distinguishing different types of built-up areas; the red band reflectance in agricultural residential spaces is generally higher than in urban residential spaces. The structural complexity of land objects helps to differentiate land classes from a different perspective. For instance, urban green spaces and non-urban green spaces have similar surface-cover characteristics, making it difficult to distinguish them based on spectral and texture features alone. However, due to human development activities, such as roads and buildings, urban green spaces exhibit a higher fragmentation and tend to have more irregular shapes. In contrast, non-urban green spaces are less affected by human activities, resulting in more regular shapes. Therefore, the structural complexity of non-urban green spaces far exceeds that of other land classes. The night-time light brightness of land patches greatly contributes to distinguishing rural residential areas from urban residential areas. As depicted in Figure 4, roads, factories, and water bodies are widely distributed, exhibiting significant variations in night-time light brightness. Conversely, urban areas have a high population density and more nocturnal production and living activities, leading to a higher night-time light brightness. In contrast, cropland and rural residential areas have lower night-time light brightness values, making it easier to differentiate between urban and rural areas.

However, certain features or combinations of features have limited discriminatory power for functional PLES types. Therefore, it is necessary to integrate multiple sources of data and consider various features using ensemble learning methods for the identification of functional PLES types.

3.2. Analysis of the Spatial Evolution Pattern of PLES in the BTH Region

The PLES spatial structure refers to the proportions of various land-use types in different areas in the study region. Changes in land-use structure can indicate future trends and help to better understand the impact of natural, economic, and population factors on land-use structure changes. This can also clarify the spatial distribution rules of PLES and promote the coordinated development of PLES land use. The PLES spatial distribution map of 2021 of the BTH region displayed in Figure 5 shows clear zonality, influenced by the Taihang Mountains running through the west of the city cluster and the Yan Mountains and the Bashang Plateau located to the north. Large areas of the western and northern regions of the study area are covered by natural ecological land such as forests and grasslands. Only some valleys and flat areas have been cultivated into farmland, with scattered villages. Covering the central and southeast areas of the BTH is the vast and flat North China Plain, most of which is used as agricultural and living space. Rural living spaces are responsible for maintaining agricultural production and are interspersed with agricultural production spaces in a sporadic manner.

The spatial distribution patterns and proportions of human-induced PLES land use (refers to the land that mainly performs the function of serving for human activities, including agricultural space, industrial space, transportation space, rural living space, urban living space, urban ecological space) in Beijing, Tianjin, and other cities in Hebei province are significantly different. Figure 6 depicts the proportion of land-cover types under artificial utilization in various cities within the Beijing–Tianjin–Hebei region. Urban

areas in Beijing and Tianjin, as megacities each with a population of over 10 million, occupy 43.67% of the urban living space within the entire urban agglomeration. The urban living space in Beijing and Tianjin is huge and concentrated, and there are extensive urban green spaces distributed throughout the city, including the central area, accounting for 17.76% and 7.95% of the urban land use, respectively. Industrial production spaces are distributed in the peripheral areas further away from the city center, indicating a high level of coordination in the PLES. In contrast, cities in the rest of Hebei are much less developed than Beijing and Tianjin, and land development and utilization are dominated by agricultural production spaces, covering approximately 6.72 million hectares of arable land in 2021, accounting for 90.17% of the arable land area of the entire BTH region and 27.17% of the total land area. In Hebei province, construction land is mainly devoted to enhancing rural living spaces, and the urban living space is relatively small in patches. The proportion of urban ecological land area is only 0.73%, and a large amount of industrial land is distributed on the edge of urban living space or even in the core area, resulting in more obvious conflicts in PLES. In general, the land in the study area is covered by natural vegetation, with non-urban ecological land and unused land accounting for 54.77% of the total area. Artificially utilized land is used for production spaces, especially for agricultural production space, accounting for 59.43% of the total area of artificially transformed land. Industrial production space and rural living space are scattered, while urban living space is mainly concentrated around several large cities. At the micro level, rural living space in plain areas is generally surrounded by agricultural production space, and a proportion of rural living areas has industrial production space distributed internally or on the periphery. Industrial production land is generally located on the outskirts of cities, but in some less developed cities in Hebei, such as Baoding, industrial production space surrounds the main urban area; there are also scattered industrial production spaces within the rural living space. Urban living space in the main urban area and some suburban centers outside the main urban area is continually expanding, gradually replacing the original "agricultural production space–rural living space" system with an "industrial production space–urban living space" system.

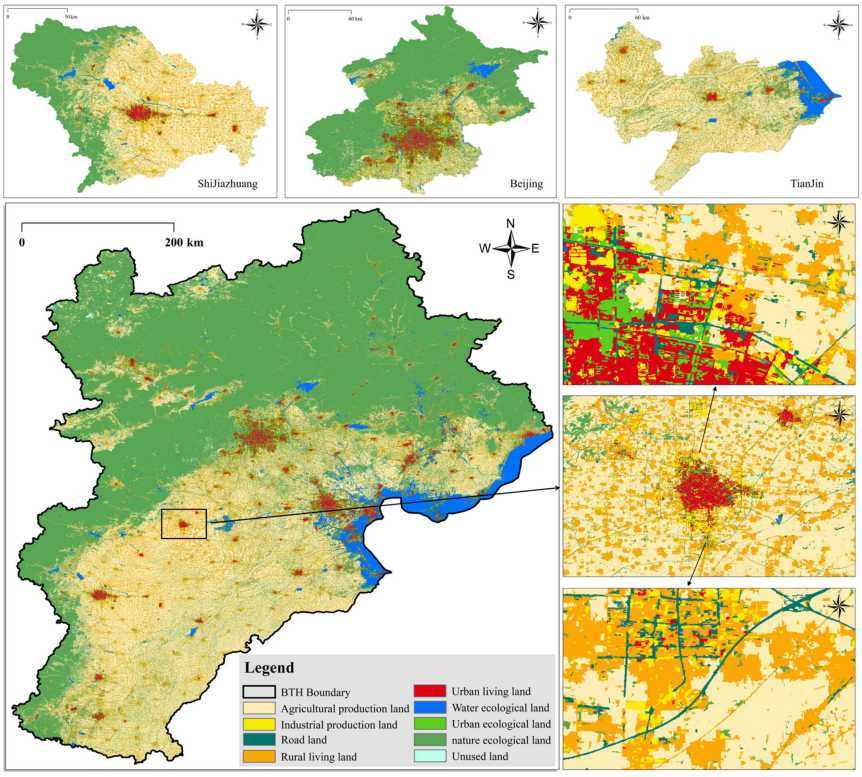

Figure 5. PLES classification results of 2021 of the BTH at different scales.

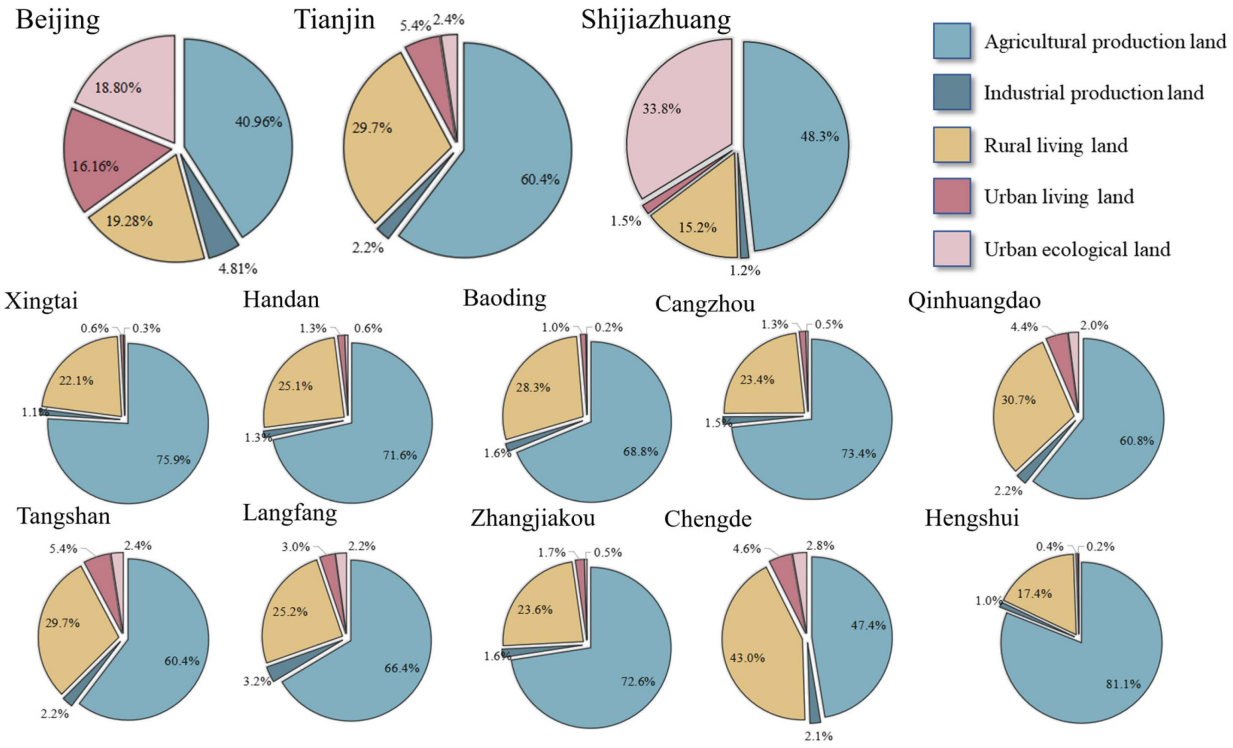

Figure 6. Distribution patterns of artificial PLES areas in different cities.

PLES in the BTH region for the years 2016 and 2021 was classified using the method and model described in the previous section. According to the classification result statistics shown in Table 4, during the 5-year period from 2016 to 2021, in the process of urbanization and industrialization in the BTH region, a small proportion of cultivated land was converted into rural living space and urban living space, resulting in a slight decrease in the overall area of cultivated land. The area of industrial production space increased slightly, but only by 0.01%, and the base area of industrial production space is relatively small; therefore, the overall area of production space slightly decreased. The changes in living space are reflected in the decrease in rural living space and the increase in urban living space, which is caused by the transformation of urban villages and village settlements on the outskirts of cities into land devoted into high-rise buildings, for example. The urban living space in Beijing and Tianjin has expanded, with a tendency towards connecting into a continuous area, while the main urban areas of other cities in Hebei, such as Shijiazhuang, are gradually becoming connected to surrounding counties to the north. Rural living space is shrinking due to the encroachment of agricultural production space and swallowing up by urban living space; however, the magnitude of this change is not significant. At the same time, due to the expansion of urban areas and the construction of urban green spaces, the area of urban ecological land has increased.

Table 4. PLES area statistics results.

PLES Type	Area in 2016 (km^2)	Area in 2021 (km^2)
Agricultural space	807.86	786.45
Industrial space	26.05	27.14
Transport space	61.42	44.46
Rural living space	280.15	267.63
Urban living space	35.13	40.02
Waters	100.99	107.37
Urban ecological space	22.17	28.89
Non-urban ecological space	1500.08	1527.95
Unused space	6.74	10.68

4. Discussion

Many scientific research teams [43–46] have been engaged in large-scale land-use classification, striving to improve the precision and accuracy of classification through finer granularity, and they have achieved meaningful results. A set of high-precision, high-availability land-use products have been produced and shared on open platforms for use by other scholars. Researchers in planning, environmental, and other fields have relied on these public data for a series of secondary classifications, exploring and summarizing the regional development laws. However, traditional large-scale land-use classification data divide the land surface into categories such as forests, cultivated land, and buildings based on the natural attributes of land cover. They do not specifically distinguish categories within buildings, which is completely inadequate for assessing the population's living environment and the sustainable development of cities, or typical regions undergoing rapid industrialization and urbanization. Therefore, this study has proposed a production–living–ecological classification system which includes nine secondary classifications, such as agricultural production space and industrial production space. Based on the functionality of land use, the classification results can facilitate fine-grained land-use analysis, providing reliable data support for the analysis of PLES in city clusters and typical regions and the sustainable development of city clusters. Figure 7 illustrates a comparison between the land-use product of the European Space Agency (ESA LUCC) [43], the land-use product of the Resource and Environmental Science Data Center of the Chinese Academy of Sciences (CNLUCC) [44], and our PLES classification product (functional PLES LUCC). As shown in Figure 7, the ESA LUCC focuses on the natural attributes of ground attachments and does not consider the fine-scale classification of different buildings. Therefore, it is not suitable for the secondary analysis of functional land use, such as production–living–ecological functions. Although the CNLUCC can distinguish between urban construction land and rural construction land, the product resolution is 30 m, which results in relatively fuzzy boundaries between different functional land parcels and prominent misclassification phenomena. In contrast, the functional PLES LUCC developed in this study has a spatial resolution of 10 m and, with the assistance of multi-source data, can differentiate between different functional types such as rural living space and urban living space. Therefore, the PLES classification dataset developed in this study has a high practicality in studies of regional development pattern evolution. And the multi-scale classification algorithm of the PLES space function in this article is applicable to both rural and urban land-use classification, taking into account both natural and artificial land-use functional characteristics. It has a wide application scope and high practical value. It needs to be emphasized in particular that, as mentioned in the introduction, the same piece of land may carry production, living, and ecological functions, and our classification system and resulting dataset focuses on identifying their dominant functions.

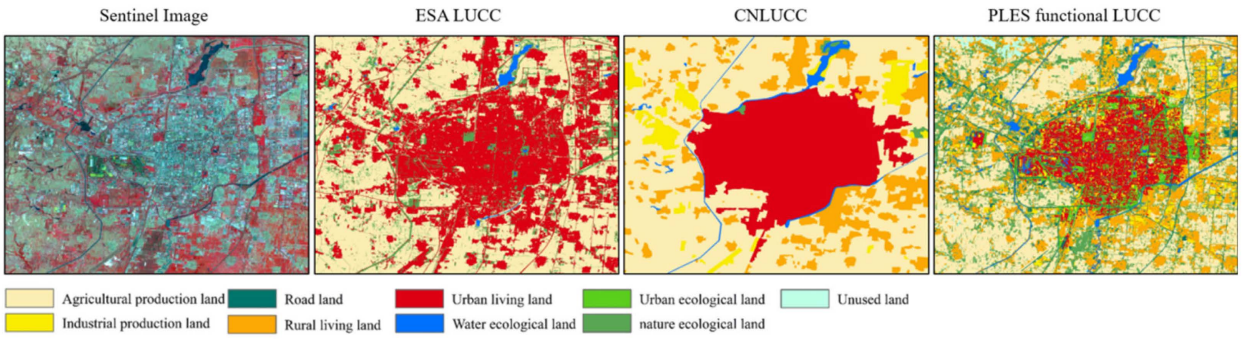

Figure 7. Comparison of our PLES classification results with other products.

However, due to the lack of strong representativeness in sample selection or insufficient sample size, the overall accuracy of the classification is limited. Moreover, this study adopted an object-oriented and multi-source data fusion spatial PLES classification

method, which required downloading remote-sensing data from the Google Earth Engine for multi-scale segmentation and multi-source data fusion. This local operation is time-consuming and laborious, rendering this method temporarily unsuitable for larger-scale land-use classification, such as at the national or global level.

In future research, facing the demand for the classification of complex urban and urban functional types, it is necessary to perform the classification of land-use functional types utilizing novel geographic big data. We will strive to select more representative samples and data sources to improve classification accuracy, improve the method system of PLES spatial classification to improve classification efficiency, and reduce data processing and classification costs to adapt our method for larger-scale classification and application.

5. Conclusions

With the rapid development of remote-sensing satellite technology, pixel-based, object-oriented, and scene-based land-use methods have gradually been formed and improved, each with their own applicable classification tasks, advantages, and disadvantages. For monitoring land-use conflicts caused by the spatial competition of PLES in the process of urbanization and industrialization, pixel-based land-use classification cannot represent the shape features and combined texture features of land cover, making it difficult to identify the functional land use; scene-based functional zone recognition has high data and computing performance requirements and is costly, which is not suitable for large-scale land-use classification. Simultaneously, the classification method based on multi-scale object-oriented segmentation can easily extract and synthesize features from complex data sources. And the object-oriented segmentation model requires a low computational performance and data resolution. Therefore, this study identified PLES in the BTH region using multi-source geographic data and an object-oriented method combined with machine-learning algorithms. The main results and conclusions are as follows.

1. Firstly, multiple-scale segmentation of the study area was performed based on remote-sensing images (Sentinel); then, the spectral, textural, shape, and socio-economic characteristics of the objects were extracted from the remote-sensing image data, night-time light data, and POI data using the segmented objects. Representative samples were selected and labeled based on the nine secondary classifications under PLES categories. These samples were used to train a random forest algorithm, which was then used to classify all the objects in the entire study area. The results showed that features extracted based on object-oriented and multi-source data can better reflect the characteristics of objects from multiple dimensions, which is effective for identifying the functional types of PLES.
2. In this study, the segmentation parameters were iteratively optimized using a multi-scale segmentation algorithm, resulting in a good segmentation effect, with the size of the segmented objects depending on the image features, and clear boundaries between different land covers. Nearly 2000 samples covering 9 second-level classifications were selected, and 11 features were extracted from multiple sources of data and used to train the random forest algorithm. The results showed that the random forest model had a strong anti-overfitting ability, could monitor the mutual influence between features, and identified small differences between different land covers. Finally, the model achieved an accuracy of 84.17% on the validation set and can thus meet the demands for large-scale land-use classification.
3. The trained model was used to identify the spatial functional PLES types of land in the BTH region in 2016 and 2021, generating a 10 m resolution spatial distribution dataset. Based on this dataset, the spatial distribution patterns and development evolution of the PLES in the BTH region were statistically analyzed. It was found that the PLES in the study area exhibited a zonal distribution. The distribution between Beijing and Tianjin and across Hebei is extremely uneven, with Beijing and Tianjin occupying a substantial proportion of the urban living space, while other cities in Hebei, such as Shijiazhuang, have more clear land-use conflicts in terms of PLES. Furthermore, this

imbalance has widened in the past 5 years. Overall, the production space in the BTH has decreased, while the living space and ecological space have increased. As the urban living space expands, urban green space also increases, and the overall layout of the PLES tends to be more reasonable.

Author Contributions: Methodology, D.J.; supervision, G.L.; writing—original draft, Z.B.; writing—review and editing, J.F. All authors have read and agreed to the published version of the manuscript.

Funding: This work was supported by a grant from the National Natural Science Foundation of China (Grant No. 41971250), State Key Laboratory of Resources and Environmental Information System, and Institute of Geographical Sciences and Natural Resources Research, Chinese Academy of Sciences (Grant No. E0V00112YZ).

Data Availability Statement: The data that support the findings of this study are available from the corresponding author upon reasonable request.

Conflicts of Interest: The authors declare no conflict of interest.

References

1. Gutman, G.; Janetos, A.C.; Justice, C.O.; Moran, E.F.; Mustard, J.F.; Rindfuss, R.R.; Skole, D.; Turner, B.L., II; Cochrane, M.A. *Land Change Science: Observing, Monitoring, and Understanding Trajectories of Change on the Earth's Surface*; Springer: Berlin/Heidelberg, Germany, 2004.
2. Chen, X.; Yu, L.; Du, Z.; Liu, Z.; Qi, Y.; Liu, T.; Gong, P. Toward sustainable land use in China: A perspective on China's national land surveys. *Land Use Policy* **2022**, *123*, 106428. [CrossRef]
3. Yang, X.; Chen, X.; Qiao, F.; Che, L.; Pu, L. Layout optimization and multi-scenarios for land use: An empirical study of production-living-ecological space in the Lanzhou-Xining City Cluster, China. *Ecol. Indic.* **2022**, *145*, 109577. [CrossRef]
4. Navin, M.S.; Agilandeeswari, L. Comprehensive review on land use/land cover change classification in remote sensing. *J. Spectr. Imaging* **2020**, *9*, a8. [CrossRef]
5. Pierdicca, N. Bayesian Techniques in Remote Sensing. *Adv. Glob. Chang. Res.* **2003**, *13*, 49–64.
6. Toth, D.; Aach, T. Improved minimum distance classification with gaussian outlier detection for industrial inspection. In Proceedings of the International Conference on Image Analysis & Processing, Palermo, Italy, 26–28 September 2001; IEEE Computer Society: Washington, DC, USA, 2001; pp. 584–588.
7. Kandrika, S.; Roy, P.S. Land use land cover classification of Orissa using multi-temporal IRS-P6 awifs data: A decision tree approach. *Int. J. Appl. Earth Obs. Geoinf.* **2008**, *10*, 186–193. [CrossRef]
8. Yuan, F.; Sawaya, K.E.; Loeffelholz, B.C.; Bauer, M.E. Land cover classification and change analysis of the Twin Cities (Minnesota) Metropolitan Area by multitemporal Landsat remote sensing. *Remote Sens. Environ.* **2005**, *98*, 317–328. [CrossRef]
9. Atkinson, P.M.; Lewis, P. Geostatistical classification for remote sensing: An introduction. *Comput. Geosci.* **2000**, *26*, 361–371. [CrossRef]
10. Khatami, R.; Mountrakis, G.; Stehman, S.V. A meta-analysis of remote sensing research on supervised pixel-based land-cover image classification processes: General guidelines for practitioners and future research. *Remote Sens. Environ.* **2016**, *177*, 89–100. [CrossRef]
11. Dorren, L.K.A.; Maier, B.; Seijmonsbergen, A.C. Improved Landsat-based forest mapping in steep mountainous terrain using object-based classification. *For. Ecol. Manag.* **2003**, *183*, 31–46. [CrossRef]
12. Peña, J.M.; Gutiérrez, P.A.; Hervás-Martínez, C.; Six, J.; Plant, R.E.; López-Granados, F. Object-based image classification of summer crops with machine learning methods. *Remote Sens.* **2014**, *6*, 5019–5041. [CrossRef]
13. Li, M.; Zang, S.Y.; Zhang, B.; Li, S.S.; Wu, C.S. A review of remote sensing image classification techniques: The role of spatio-contextual information. *Eur. J. Remote Sens.* **2014**, *47*, 389–411. [CrossRef]
14. Hussain, M.; Chen, D.; Cheng, A.; Wei, H.; Stanley, D. Change detection from remotely sensed images: From pixel-based to object-based approaches. *ISPRS J. Photogramm. Remote Sens.* **2013**, *80*, 91–106. [CrossRef]
15. Moskal, L.M.; Styers, D.M.; Halabisky, M. Monitoring urban tree cover using object-based image analysisand public domain remotely sensed data. *Remote Sens.* **2011**, *3*, 2243–2262. [CrossRef]
16. Li, M.; Bijker, W.; Stein, A. Use of binary partition tree and energy minimization for object-based classification of urban land cover. *ISPRS J. Photogramm. Remote Sens.* **2015**, *102*, 48–61. [CrossRef]
17. Yin, J.; Dong, J.; Hamm, N.A.; Li, Z.; Wang, J.; Xing, H.; Fu, P. Integrating remote sensing and geospatial big data for urban land use mapping: A review. *Int. J. Appl. Earth Obs. Geoinf.* **2021**, *103*, 102514. [CrossRef]
18. Memon, N.; Parikh, H.; Patel, S.B.; Patel, D.; Patel, V.D. Automatic land cover classification of multi-resolution dualpol data using convolutional neural network (CNN). *Remote Sens. Appl. Soc. Environ.* **2021**, *22*, 100491. [CrossRef]
19. Bao, H.; Ming, D.; Guo, Y.; Zhang, K.; Zhou, K.; Du, S. DFCNN-based semantic recognition of urban functional zones by integrating remote sensing data and POI data. *Remote Sens.* **2020**, *12*, 1088. [CrossRef]

20. Chang, S.; Wang, Z.; Mao, D.; Guan, K.; Jia, M.; Chen, C. Mapping the essential urban land use in changchun by applying random forest and multi-source geospatial data. *Remote Sens.* **2020**, *12*, 2488. [CrossRef]
21. Hu, T.; Yang, J.; Li, X.; Gong, P. Mapping urban land use by using landsat images and open social data. *Remote Sens.* **2016**, *8*, 151. [CrossRef]
22. Zhang, S.; Li, C.; Sun, J.; Wang, J. Identification of Urban Functional Zones Using High-Resolution Remote Sensing Images and Socioeconomic Big Data. *ISPRS Int. J. Geo-Inf.* **2021**, *10*, 242.
23. Zhang, X.; Du, S.; Wang, Q. Hierarchical semantic cognition for urban functional zones with VHR satellite images and POI data. *ISPRS J. Photogramm. Remote Sens.* **2017**, *132*, 170–184. [CrossRef]
24. Feng, Y.; Huang, Z.; Wang, Y.; Wan, L.; Liu, Y.; Zhang, Y.; Shan, X. An SOE-Based Learning Framework Using Multisource Big Data for Identifying Urban Functional Zones. *IEEE J. Sel. Top. Appl. Earth Obs. Remote Sens.* **2021**, *14*, 7336–7348. [CrossRef]
25. Kamusoko, C.; Kamusoko, O.W.; Chikati, E.; Gamba, J. Mapping urban and peri-urban land cover in Zimbabwe: Challenges and opportunities. *Geomatics* **2021**, *1*, 114–147. [CrossRef]
26. Bruzzone, L.; Demir, B. A review of modern approaches to classification of remote sensing data. *Land Use Land Cover. Mapp. Eur. Pract. Trends* **2014**, *18*, 127–143.
27. Zhang, H.B.; Li, M.H.; Zhang, Q.L. Construction of land classification system and land type identification for territorial spatial planning based on multi-source data. *Trans. Chin. Soc. Agric. Eng.* **2020**, *36*, 261–269.
28. Jin, X.; Lu, Y.; Lin, J.; Qi, X.; Hu, G.; Li, X. Research on the evolution of spatiotemporal patterns of production-living-ecological space in an urban agglomeration in the Fujian Delta region, China. *Acta Ecol. Sin.* **2018**, *38*, 4286–4295.
29. Liu, J.L.; Liu, Y.S.; Li, Y.R.; Liu, J.L.; Liu, Y.S.; Li, Y.R. Classification evaluation and spatial-temporal analysis of "production-living-ecological" spaces in China. *Acta Geogr. Sin.* **2017**, *72*, 1290–1304.
30. Lin, J.; Wu, Y.X.; Wu, J.Y. Construction of the spatial planning system: With discussions on the relationship between spatial planning, territorial spatial regulation, and natural resources supervision. *City Plan. Rev.* **2018**, *42*, 9–17.
31. Ji, Z.X.; Liu, C.; Xu, Y.Q.; Huang, A.; Lu, L.H.; Duan, Y.M. Identification and optimal regulation of the production-living-ecological space based on quantitative land use functions. *Trans. Chin. Soc. Agric. Eng.* **2020**, *36*, 222–231.
32. Fu, J.; Bu, Z.; Jiang, D.; Lin, G.; Li, X. Sustainable land use diagnosis based on the perspective of production–living–ecological spaces in China. *Land Use Policy* **2022**, *122*, 106386. [CrossRef]
33. Li, G.D.; Fang, C.L. Quantitative function identification and analysis of urban ecological-production-living spaces. *Acta Geogr. Sin.* **2016**, *71*, 49–65.
34. Xia, N.; Hai, W.; Tang, M.; Song, J.; Quan, W.; Zhang, B.; Ma, Y. Spatiotemporal evolution law and driving mechanism of production–living–ecological space from 2000 to 2020 in Xinjiang, China. *Ecol. Indic.* **2023**, *154*, 110807. [CrossRef]
35. Fu, C.; Tu, X.; Huang, A. Identification and characterization of Production–living–ecological space in a central urban area based on POI data: A case study for Wuhan, China. *Sustainability* **2021**, *13*, 7691. [CrossRef]
36. Hao, L.; Yu, J.; Du, C.; Wang, P. A policy support framework for the balanced development of economy-society-water in the Beijing-Tianjin-Hebei urban agglomeration. *J. Clean. Prod.* **2022**, *374*, 134009. [CrossRef]
37. Wang, Y.; Xie, Y.; Qi, L.; He, Y.; Bo, H. Synergies evaluation and influencing factors analysis of the water–energy–food nexus from symbiosis perspective: A case study in the Beijing–Tianjin–Hebei region. *Sci. Total Environ.* **2022**, *818*, 151731. [CrossRef] [PubMed]
38. Cui, Y. The coordinated relationship among industrialization, environmental carrying capacity and green infrastructure: A comparative research of Beijing-Tianjin-Hebei region, China. *Environ. Dev.* **2022**, *44*, 100775. [CrossRef]
39. Zheng, Y.; Tang, L.; Wang, H. An improved approach for monitoring urban built-up areas by combining NPP-VIIRS nighttime light, NDVI, NDWI, and NDBI. *J. Clean. Prod.* **2021**, *328*, 129488. [CrossRef]
40. Jiang, S.; Alves, A.; Rodrigues, F.; Ferreira, J., Jr.; Pereira, F.C. Mining point-of-interest data from social networks for urban land use classification and disaggregation. *Comput. Environ. Urban Syst.* **2015**, *53*, 36–46. [CrossRef]
41. Fathizad, H.; Ardakani, M.A.H.; Mehrjardi, R.T.; Sodaiezadeh, H. Evaluating desertification using remote sensing technique and object-oriented classification algorithm in the Iranian central desert. *J. Afr. Earth Sci.* **2018**, *145*, 115–130. [CrossRef]
42. Carbonell, J.G.; Michalski, R.S.; Mitchell, T.M. Machine learning: A historical and methodological analysis. *AI Mag.* **1983**, *4*, 69.
43. Zanaga, D.; Van De Kerchove, R.; Daems, D.; De Keersmaecker, W.; Brockmann, C.; Kirches, G.; Wevers, J.; Cartus, O.; Santoro, M.; Fritz, S.; et al. ESA WorldCover 10 m 2021 v200. 2022. Available online: https://zenodo.org/records/7254221 (accessed on 20 February 2023).
44. Xu, X.; Liu, J.; Zhang, S.; Li, R.; Yan, C.; Wu, S. *China's Multi-Period Land Use Land Cover Remote Sensing Monitoring Data Set (CNLUCC)*; Resource and Environment Data Cloud Platform: Beijing, China, 2018.
45. Rosier, J.F.; Taubenböck, H.; Verburg, P.H.; van Vliet, J. Fusing Earth observation and socioeconomic data to increase the transferability of large-scale urban land use classification. *Remote Sens. Environ.* **2022**, *278*, 113076. [CrossRef]
46. Zhang, X.; Liu, L.; Wang, Y.; Hu, Y.; Zhang, B. A SPECLib-based operational classification approach: A preliminary test on China land cover mapping at 30 m. *Int. J. Appl. Earth Obs. Geoinf.* **2018**, *71*, 83–94. [CrossRef]